Global Ocean Studies from ICESat-2 mission

Xiaomei Lu
Lidar Science Branch, Science Directorate
NASA Langley Research Center
Hampton, VA, USA
xiaomei.lu@nasa.gov

Yongxiang Hu
Lidar Science Branch, Science Directorate
NASA Langley Research Center
Hampton, VA, USA
yongxiang.hu-1@nasa.gov

Ali Omar
Lidar Science Branch, Science Directorate
NASA Langley Research Center
Hampton, VA, USA
ali.h.omar@nasa.gov

Yuekui Yang
Climate and Radiation Lab.,
NASA Goddard Space Flight Center
Greenbelt, MD, USA
yuekui.yang-1@nasa.gov

Laura Rogers
Lidar Science Branch, Science Directorate
NASA Langley Research Center
Hampton, VA, USA
laura.j.rogers@nasa.gov

***Abstract*—The primary purpose of ICESat-2 mission is to monitor changes in the cryosphere. Fortunately, additional, and unrealized information from the penetration of laser light below ocean surface offers a new and exciting opportunity to study the ocean biology globally. The objective of this study is to provide the global ocean subsurface results (e.g., depolarization ratio and particulate backscattering coefficient) from ATLAS/ICESat-2 lidar measurements. The seasonal maps of ATLAS retrieved subsurface results exhibit all the major ocean plankton features anticipated from the earlier passive ocean color and CALIOP/CALIPSO lidar measurements. The ICESat-2 ATLAS lidar can continue to monitor global ocean phytoplankton properties after CALIOP/CALIPSO mission. Moreover, the ICESat-2 ocean subsurface results provide unique information to augment existing ocean color measurements by adding nighttime observations and the depth dimension with high horizontal and vertical resolutions.**

Keywords—ICESat-2, CALIPSO, Ocean, Space Lidar, Phytoplankton, particulate backscattering coefficient.

I. INTRODUCTION

Global ocean plankton retrievals from a space-based lidar were first demonstrated using measurements from the Cloud-Aerosol Lidar with Orthogonal Polarization (CALIOP) sensor [1], which is a dual-wavelength (532 nm and 1064 nm), polarization sensitive (at 532 nm) elastic backscatter lidar [1]. CALIOP is the primary instrument on the Cloud-Aerosol Lidar and Infrared Pathfinder Satellite Observation (CALIPSO) satellite and has been making measurements between 82°S and 82°N since June 2006 [1,2]. Although CALIOP was designed for atmospheric profiles of aerosols and clouds applications, its measurements over the Earth's oceans provide a wealth of unanticipated opportunities for ocean biology and biogeochemistry studies [3–5]. During the last decade, innovative retrieval methods have been developed to translate CALIOP's ocean backscattered signals into ocean optical properties such as global phytoplankton distributions [3], total particulate organic carbon (POC) stocks [3,6], particulate backscattering coefficients (b_{bp}, m^{-1}) [7–10], phytoplankton biomass [4], and depolarization ratio of ocean waters [11–14]. Those breakthroughs have demonstrated the satellite lidar era in the oceanography has arrived [15–17].

The CALIPSO mission is entering its 17th year of very successful operation, providing the first decadal dataset of global ocean observations during both daytime and nighttime [4,5], which are critical to global ocean biology studies and phytoplankton model improvements. However, the CALIPSO mission will be soon decommissioned (~September 2023). Stable, long-term time series of satellite lidar ocean observations are critical to the ongoing investigation and understanding of the global ocean biomass. Fortunately, NASA has launched the Ice, Cloud, and land Elevation Satellite-2 (ICESat-2) mission in September 2018 [18–20]. The sole instrument onboard ICESat-2 satellite is Advanced Topographic Laser Altimeter System (ATLAS), which is a green (at 532 nm) photon counting lidar with a 10 kHz pulse repetition rate, a footprint diameter of ~11 m, and an along-track sampling interval of 0.7 m at the Earth's surface [21,22]. ATLAS has been making measurements between 88°S and 88°N since October 2018, providing useful satellite lidar dataset to overlap with CALIOP dataset. The overlapped dataset from these two space lidars offer an opportunity for intercomparisons between the two instruments.

In this study, we present an approach to estimate the global ocean depolarization ratio (δ), and particulate backscattering coefficients (b_{bp}, m^{-1}) from ATLAS measured subsurface photons in order to develop a stable, long-term time series of global ocean dataset from both CALIOP and ATLAS space lidars. The ICESat-2 ATLAS retrieved ocean subsurface optical properties (δ and b_{bp}) are then evaluated using the corresponding overlapped CALIOP ocean results. Compared with CALIOP lidar that provide measurements at ~70 m footprint every 333 m along the ground track [2], ICESat-2 ATLAS lidar has the advantage of providing measurements from six individual beams with a smaller footprint and smaller along track sampling interval [23].

This study is organized as follows. In Section II we present the ATLAS and CALIOP data products used in this paper. The ATLAS observed global ocean subsurface photons and the new retrieval method are given in Section III. The ATLAS retrieved global ocean results and their comparisons with CALIOP results are presented in Section IV. Finally, a brief conclusion is provided in Section V.

II. ATLAS AND CALIOP DATA

The primary purpose of ICESat-2 mission is to monitor changes in the cryosphere [18]. Many other areas of Earth science are also benefit from the ICESat-2 mission: the atmospheric community has access to the derived atmospheric and cloud properties [24]; the hydrological community is provided with global inland water body height and associated properties [25]; the oceanography community is given global ocean and wave heights [26], as well as snow thickness [27–29] and permafrost monitoring. In addition, the ICESat-2 ATLAS detected photons over global oceans provide great opportunity for studying the ocean subsurface optical properties and their vertical structures [10,30,31].

In this work, we use version 5 of ICESat-2 ATL03 geolocated photon data [32] and CALIOP Level 1 (L1) version 4.1 data products [33,34] from October 2018 to November 2020 during nighttime. The ATL03 product publicly available through NSIDC [35] was designed to be a single source for all photon data and ancillary information (e.g., the ATLAS impulse response function) required by one or more higher-level data products [36]. The calibration of the attenuated backscatter coefficients at 532 nm from CALIOP L1 version 4.1 product is significantly improved with respect to previous versions [37,38].

ATLAS measured ocean cases with surface photon counts between 1 and 12 per pulse are selected. Cases for which the ocean surface return is greater than 12 counts/pulse or less than 1 count/pulse are removed in the retrieval process due to possible saturation from specular reflection and low signal-to-noise ratio, respectively [39]. The returned signal from ocean surface *S(0)* at zero meter and subsurface *S(z)* at water depth z can be written as:

$$S(0) = A\beta_{surface}T_{atm}^2 \quad (1)$$

$$S(z) = A\beta_{sub}(z)T_w^2T_{atm}^2 \quad (2)$$

Where A is the lidar system calibration constant, $\beta_{surface}$ and $\beta_{sub}(z)$ are ocean surface and subsurface backscattering coefficient, T_{atm}^2 and T_w^2 are atmospheric and water column two-way transmittances, respectively, z is the water depth below ocean surface. The calibrated subsurface attenuated backscatter (β') is:

$$\beta'(z) = \beta_{sub}(z)T_w^2 = R(z)\beta_{surface} \quad (3)$$

$$R(z) = \frac{S(z)}{S(0)} \quad (4)$$

R(z) is the ATLAS observed subsurface photon ratio profile (or calibrated subsurface photon) between subsurface photon counts at water depth z and ocean surface photon counts at zero meter. The calibrated subsurface attenuated backscatter and subsurface photons in Eqs. (3) and (4) remove the effects from the atmospheric attenuation (T_{atm}^2) and lidar system calibration constant (A) easily and accurately because the laser light passed through the same atmospheric column and the lidar system when backscattered from the ocean surface and then the subsurface.

One of the major challenges for passive ocean color remote sensing is accurately accounting for atmospheric contributions to the measured top-of-atmosphere radiances [40]. This atmospheric correction issue (e.g., T_{atm}^2) for the determination of ocean properties is largely eliminated in space lidar (e.g., ATLAS) retrievals because atmosphere signals, ocean surface, and subsurface signals are separated in time (or photon heights), allowing equivalent retrieval accuracies under clear sky, cloudy, or heavy-aerosol-load conditions. To retrieve the ocean properties from spaceborne lidar measurements, atmospheric attenuation (T_{atm}^2) and lidar system calibration constant (A) can be easily calibrated through a comparison of lidar measured ocean surface signals and the theoretical ocean surface backscatter ($\beta_{surface}$) at 532 nm [30,31]. The theoretical ocean surface backscatter ($\beta_{surface}$) can be estimated from wind speed [41,42]. In this study, the 10 meters above ocean surface wind speed from Advanced Microwave Scanning Radiometer (AMSR-2) monthly data products (Version 8.2) [43] are used to estimate the ocean surface backscatter $\beta_{surface}$.

III. Neural Network Method

A. ATLAS global ocean subsurface photons

The ATLAS observed calibrated subsurface attenuated backscatter and subsurface photons (Eq. 3 and 4) is a function of water properties such as water column optical depth, backscattering coefficient. They are independent of atmospheric attenuation of T_{atm}^2 and lidar system calibration constant A as shown in Eq. 3 and 4. For example, Fig. 1 shows the seasonal distributions of ATLAS observed calibrated subsurface photon ratios *R(4m)* at 4 m below ocean surface during nighttime. The atmospheric contributions (two-way transmittance) and system constant are easily and accurately removed by the photon ratios as shown in Eq. (4).

The global subsurface photons shown in Fig. 1 exhibits all the major ocean plankton features anticipated from both the passive ocean color and CALIOP lidar ocean results. The low values (<1.6%) of *R(4m)* over most of the permanently stratified oceans roughly 40°S ~40°N are stable over the annual cycle, indicating low nutrient, low biomass waters, except in coastal regions and the Eastern Pacific upwelling regions (latitude: 0°~20°S, longitude: 80°W~ 160°W). The seasonal changes of *R(4m)* illustrate the strong seasonality of high latitude phytoplankton communities. For example, the elevated *R(4m)* values (>2%) in the subarctic oceans reflect the large boreal summer and fall phytoplankton blooms (Fig. 1b and 1c), while *R(4m)* in the Southern Oceans reflect the large austral summer bloom (Fig. 1d). Results of Fig. 1 indicates that the ATLAS observed subsurface photons can be used for global ocean optical properties retreivals.

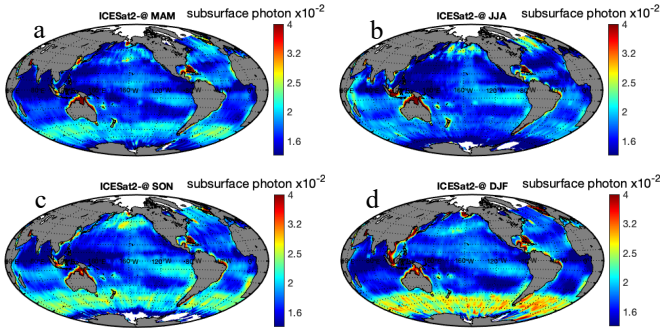


Fig. 1. Seasonal distributions of ATLAS observed photon ratio R(4m) between subsurface photons 4 m below surface and ocean surface photons during nighttime: (a) March-May; (b) June-August; (c) September-November; and (d) December-February. Data are seasonally averaged climatologies for the 2018-2020 period binned to 1° latitude by 1° longitude pixels.

B. Neural Network method

Previous studies indicate that the CALIOP depolarization ratio (δ) at 532 nm provides valuable information about ocean phytoplankton distributions [3,7,10–14]. The depolarization ratio is a fundamental parameter that can be used as the input for high-level ocean properties retrievals, such as particulate backscattering coefficient [10]. For this study, the CALIOP depolarization ratio (δ) at 532 nm after removing crosstalk are used [14].

Figure 2(a) shows an example of relationship between and CALIOP depolarization ratio (y-axis) and ATLAS subsurface photons at 4 m below ocean surface (x-axis). The color represents the density of the collocated ATLAS and CALIOP '*R(4m) -δ*' data points within 1°×1° latitude and longitude grid. Note the relationship in Fig. 2(a) was only for ATLAS subsurface photons 4 m below ocean surface, it can be changed for subsurface photons at different water depths with different water optical properties. However, Fig. 2(a) still demonstrated that there are relationships between ATLAS subsurface photons and CALIOP depolarization ratio.

With the advancement in computer technology, an artificial neural network (NN) has the capacity to handle the nonlinear relationships and learn weights that map any input to the output. Here, a NN algorithm is proposed to estimate the global ocean depolarization ratio from ATLAS observed subsurface photons. The schematic chart of the NN is given in Fig. 2(b), where the ATLAS observed subsurface photon profiles with their geolocations (e.g., latitude and longitude) and the theoretical ocean surface backscatter ($\beta_{surface}$) are used as the input for NN and the CALIOP depolarization ratio is as the output. A reliable NN algorithm requires a large training dataset with a wide range of water optical properties. In this study, the collocated results of ATLAS global ocean subsurface photon profiles *R(z)* from 3 m to 10 m below ocean surface and CALIOP global ocean depolarization ratio from Oct 2018 to Nov 2020 during nighttime were selected to train the NN algorithm. The subsurface photon counts 15 m below ocean surface are not selected due to the fact that they were usually reduced by the ICESat-2 telemetry window that is used to limit the amount of data sent to downlink stations. More details about the ATLAS and CALIOP data analyses by removing each lidar system's artifacts can be founded in [10]. We subdivided the training dataset into subsets of 80/20 training/testing to perform the NN model accuracy assessment. The trained NN model was then applied to all available ATLAS data over global oceans.

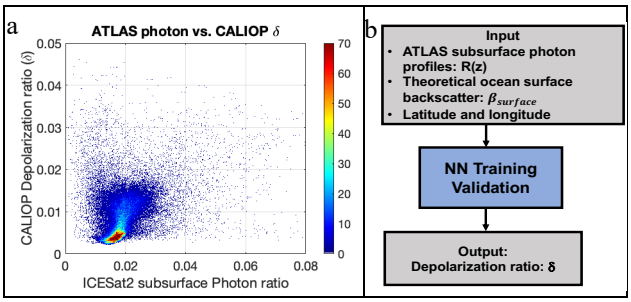


Fig. 2. Left panel: relationship between ATLAS photon ratio at 4 m and CALIOP depolarization ratio (δ). Right panel: schematic chart of the neural network (NN) algorithm for the estimation of depolarization ratio from ATLAS observed subsurface photons.

IV. Results and Intercomparison

Figure 3 shows the seasonal distributions of the ATLAS retrieved global ocean depolarization ratio by NN algorithm. The color represents the values of δ. Then, the ATLAS particulate backscattering coefficient b_{bp} can be estimated from the ocean depolarization ratio based on previous published methods [3,10,14]. The seasonal variations of ATLAS retrieved δ and b_{bp} results from subarctic oceans, to coastal areas, and to Southern Oceans can be clearly seen in Figs. 3 and 4, indicating the new NN algorithm was successfully trained over global oceans, although future upgrades and revisions with more overlapped ATLAS and CALIOP datasets during both daytime and nighttime are necessary in algorithm development.

The comparisons between ATLAS retrieved monthly δ results (x-axis) and CALIOP retrieved monthly δ results (y-axis) is showing in Fig. 5(a). The ATLAS retrieved δ results in the range of 0.01% - 6.35% agree very well with CALIOP results. Most of the matched ATLAS and CALIOP δ results are around the 1:1 line with coefficient of determination (R^2) of 0.73 and root mean square error (RMSE) as 0.22%. The corresponding b_{bp} comparisons between the two space lidars are shown in Fig. 5(b) with R^2 of 0.58 and RMSE of 0.91×10^{-3} m^{-1}. The comparisons of Fig. 5 indicates consistent global ocean δ and b_{bp} products can be generated from the two independent space lidars, which provide a wealth of unique information (e.g., nighttime results shown in Figs. 3 and 4) to complement existing satellite-based passive ocean color remote sensing capabilities, which only provide ocean color records during daytime and is limited to the very upper water column and is unable to resolve the vertical structures of the oceans.

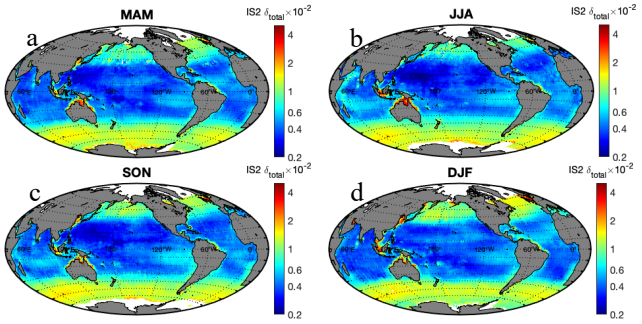


Fig. 3. Seasonal distributions of ATLAS retrieved depolarization ratios (δ) during nighttime: (a) March-May; (b) June-August; (c) September-November; and (d) December-February. Data are seasonally averaged climatologies binned to 1° latitude by 1° longitude pixels.

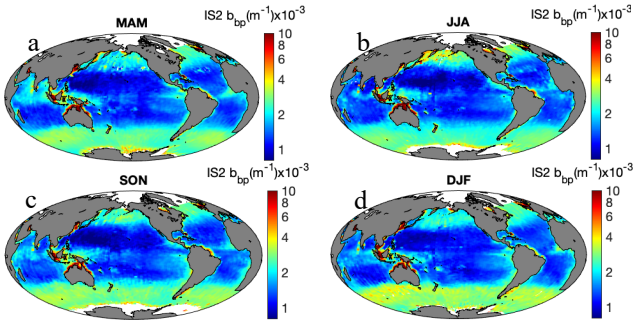


Fig. 4. Seasonal distributions of ATLAS retrieved particulate backscattering coefficient (b_{bp}) during nighttime: (a) March-May; (b) June-August; (c) September-November; and (d) December-February. Data are seasonally averaged climatologies binned to 1° latitude by 1° longitude pixels.

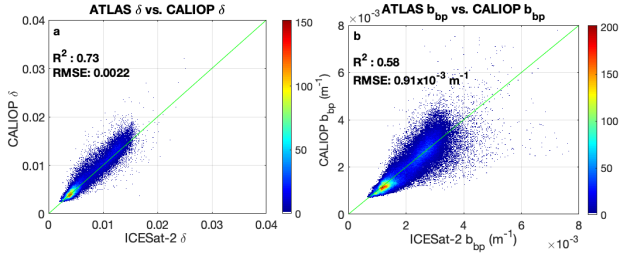


Fig. 5. Left panel: Comparison between ATLAS retrieved δ (x-axis) and CALIOP retrieved δ (y-axis). Right panel: Comparison between ATLAS

retrieved b_{bp} (x-axis) and CALIOP retrieved b_{bp} (y-axis). The green lines are the 1:1 lines, and the color represents the density of the matched ATLAS and CALIOP data points during nighttime measurements.

V. Conclusions

Within this study, a NN-based algorithm was proposed to retrieve global ocean subsurface properties of depolarization ratio and particulate backscattering coefficient from ICESat-2 ATLAS lidar measurements. With the overlapped and collocated measurements from two space-based lidars: ATLAS/ICESat-2 and CALIOP/CALIPSO, the NN model has been established on a large training data matchup covering a wide range of water properties. The calibrated ATLAS subsurface photon profiles were used as an input and the CALIOP retrieved depolarization ratio as the output. The NN model was applied to available ATLAS measurements over global oceans during nighttime to retrieve the depolarization ratio. The particulate backscattering coefficient can be finally retrieved from the depolarization ratio results based on previous published CALIOP processing approaches.

Results presented here demonstrate that the ICESat-2 ATLAS lidar can continue to monitor global ocean phytoplankton properties when CALIOP/CALIPSO lidar will be decommissioned in near future. Stable, long-term time series of global ocean dataset are expected to be developed from CALIPSO and ICESat-2 missions. The satellite passive ocean color measurements require sunlight and are compromised when solar viewing angles are steep. As a result, the passive ocean color has no information on plankton properties at night and yields little information on polar ecosystems, especially over polar night. The merged CALIPSO and ICESat-2 global ocean products over the past decade provide a wealth of unique information for global ocean biology studies and their responses to climate changes.

Acknowledgment

The CALIPSO V4 lidar level 1B profile data used in this study can be freely accessed via https://doi.org/10.5067/CALIOP/CALIPSO/LID_L1-STANDARD-V4-10. The ICESat-2 geolocated photon data (ATL03 Release 005) are publicly available through the National Snow and Ice Data Center (NSIDC). AMSR data are produced by Remote Sensing Systems and sponsored by NASA. We are grateful to JAXA for providing AMSR source data. Funding for the lead author was provided by the NASA awards [grant numbers 80NSSC20K0129 and 80NSSC21K0910] for CALIPSO and ICESat-2 projects

References

[1] D. M. Winker, M. A. Vaughan, A. Omar, Y. Hu, K. A. Powell, Z. Liu, W. H. Hunt, and S. A. Young, "Overview of the CALIPSO Mission and CALIOP Data Processing Algorithms," J. Atmospheric Ocean. Technol. 26(11), 2310–2323 (2009).

[2] W. H. Hunt, D. M. Winker, M. A. Vaughan, K. A. Powell, P. L. Lucker, and C. Weimer, "CALIPSO Lidar Description and Performance Assessment," J. Atmospheric Ocean. Technol. 26(7), 1214–1228 (2009).

[3] M. J. Behrenfeld, Y. Hu, C. A. Hostetler, G. Dall'Olmo, S. D. Rodier, J. W. Hair, and C. R. Trepte, "Space-based lidar measurements of global ocean carbon stocks," Geophys. Res. Lett. 40(16), 4355–4360 (2013).

[4] M. J. Behrenfeld, Y. Hu, R. T. O/'Malley, E. S. Boss, C. A. Hostetler, D. A. Siegel, J. L. Sarmiento, J. Schulien, J. W. Hair, X. Lu, S. Rodier, and A. J. Scarino, "Annual boom-bust cycles of polar phytoplankton biomass revealed by space-based lidar," Nat. Geosci 10(2), 118–122 (2017).

[5] M. J. Behrenfeld, P. Gaube, A. Della Penna, R. T. O'Malley, W. J. Burt, Y. Hu, P. S. Bontempi, D. K. Steinberg, E. S. Boss, D. A. Siegel, C. A. Hostetler, P. D. Tortell, and S. C. Doney, "Global satellite-observed daily vertical migrations of ocean animals," Nature 576(7786), 257–261 (2019).

[6] X. Lu and Y. Hu, "Estimation of particulate organic carbon in the ocean from space-based polarization lidar measurements," in (2014), 9261, pp. 92610Z-92610Z–8.

[7] L. Lacour, R. Larouche, and M. Babin, "In situ evaluation of spaceborne CALIOP lidar measurements of the upper-ocean particle backscattering coefficient," Opt. Express 28(18), 26989–26999 (2020).

[8] X. Lu, Y. Hu, J. Pelon, C. Trepte, K. Liu, S. Rodier, S. Zeng, P. Lucker, R. Verhappen, J. Wilson, C. Audouy, C. Ferrier, S. Haouchine, B. Hunt, and B. Getzewich, "Retrieval of ocean subsurface particulate backscattering coefficient from space-borne CALIOP lidar measurements," Opt. Express 24(25), 29001–29008 (2016).

[9] K. M. Bisson, E. Boss, P. J. Werdell, A. Ibrahim, and M. J. Behrenfeld, "Particulate Backscattering in the Global Ocean: A Comparison of Independent Assessments," Geophys. Res. Lett. 48(2), e2020GL090909 (2021).

[10] X. Lu, Y. Hu, Y. Yang, T. Neumann, A. Omar, R. Baize, M. Vaughan, S. Rodier, B. Getzewich, P. Lucker, C. Trepte, C. Hostetler, and D. Winker, "New Ocean Subsurface Optical Properties From Space Lidars: CALIOP/CALIPSO and ATLAS/ICESat-2," Earth Space Sci. 8(10), e2021EA001839 (2021).

[11] D. Dionisi, V. E. Brando, G. Volpe, S. Colella, and R. Santoleri, "Seasonal distributions of ocean particulate optical properties from spaceborne lidar measurements in Mediterranean and Black sea," Remote Sens. Environ. 247, 111889 (2020).

[12] X. Lu, Y. Hu, C. Trepte, S. Zeng, and J. H. Churnside, "Ocean subsurface studies with the CALIPSO spaceborne lidar," J. Geophys. Res. Oceans 119(7), 4305–4317 (2014).

[13] J. Churnside, B. McCarty, and X. Lu, "Subsurface Ocean Signals from an Orbiting Polarization Lidar," Remote Sens. 5(7), 3457–3475 (2013).

[14] X. Lu, Y. Hu, A. Omar, R. Baize, M. Vaughan, S. Rodier, J. Kar, B. Getzewich, P. Lucker, C. Trepte, C. Hostetler, and D. Winker, "Global Ocean Studies from CALIOP/CALIPSO by Removing Polarization Crosstalk Effects," Remote Sens. 13(14), (2021).

[15] C. A. Hostetler, M. J. Behrenfeld, Y. Hu, J. W. Hair, and J. A. Schulien, "Spaceborne Lidar in the Study of Marine Systems," Annu. Rev. Mar. Sci. 10(1), 121–147 (2018).

[16] C. Jamet, A. Ibrahim, Z. Ahmad, F. Angelini, M. Babin, M. J. Behrenfeld, E. Boss, B. Cairns, J. Churnside, J. Chowdhary, A. B. Davis, D. Dionisi, L. Duforêt-Gaurier, B. Franz, R. Frouin, M. Gao, D. Gray, O. Hasekamp, X. He, C. Hostetler, O. V. Kalashnikova, K. Knobelspiesse, L. Lacour, H. Loisel, V. Martins, E. Rehm, L. Remer, I. Sanhaj, K. Stamnes, S. Stamnes, S. Victori, J. Werdell, and P.-W. Zhai, "Going Beyond Standard Ocean Color Observations: Lidar and Polarimetry," Front. Mar. Sci. 6, 251 (2019).

[17] J. H. Churnside and J. A. Shaw, "Lidar remote sensing of the aquatic environment: invited," Appl. Opt. 59(10), C92–C99 (2020).

[18] T. Markus, T. Neumann, A. Martino, W. Abdalati, K. Brunt, B. Csatho, S. Farrell, H. Fricker, A. Gardner, D. Harding, M. Jasinski, R. Kwok, L. Magruder, D. Lubin, S. Luthcke, J. Morison, R. Nelson, A. Neuenschwander, S. Palm, S. Popescu, C. Shum, B. E. Schutz, B. Smith, Y. Yang, and J. Zwally, "The Ice, Cloud, and land Elevation Satellite-2 (ICESat-2): Science requirements, concept, and implementation," Remote Sens. Environ. 190, 260–273 (2017).

[19] S. C. Popescu, T. Zhou, R. Nelson, A. Neuenschwander, R. Sheridan, L. Narine, and K. M. Walsh, "Photon counting LiDAR: An adaptive ground and canopy height retrieval algorithm for ICESat-2 data," Remote Sens. Environ. 208, 154–170 (2018).

[20] A. Neuenschwander and K. Pitts, "The ATL08 land and vegetation product for the ICESat-2 Mission," Remote Sens. Environ. 221, 247–259 (2019).

[21] L. Magruder, K. Brunt, and M. Alonzo, "Early ICESat-2 on-orbit Geolocation Validation Using Ground-Based Corner Cube Retro-Reflectors," Remote Sens. 12, 3653 (2020).

[22] L. Magruder and K. Brunt, "Performance Analysis of Airborne Photon-Counting Lidar Data in Preparation for the ICESat-2 Mission," IEEE Trans. Geosci. Remote Sens. 56(5), 2911–2918 (2018).

[23] T. A. Neumann, A. J. Martino, T. Markus, S. Bae, M. R. Bock, A. C. Brenner, K. M. Brunt, J. Cavanaugh, S. T. Fernandes, D. W. Hancock, K. Harbeck, J. Lee, N. T. Kurtz, P. J. Luers, S. B. Luthcke, L.

Magruder, T. A. Pennington, L. Ramos-Izquierdo, T. Rebold, J. Skoog, and T. C. Thomas, "The Ice, Cloud, and Land Elevation Satellite – 2 mission: A global geolocated photon product derived from the Advanced Topographic Laser Altimeter System," Remote Sens. Environ. 233, 111325 (2019).

[24] S. Palm, Y. Yang, U. Herzfeld, D. Hancock, K. A. Barbieri, J. Wimert, and the ICESat-2 Science Team, "ATLAS/ICESat-2 L3A Calibrated Backscatter Profiles and Atmospheric Layer Characteristics, Version 1," Boulder Colo. USA NASA Natl. Snow Ice Data Cent. Distrib. Act. Arch. Cent. (2019).

[25] M. F. Jasinski, J. D. Stoll, W. B. Cook, M. Ondrusek, E. Stengel, and K. Brunt, "Inland and Near-Shore Water Profiles Derived from the High-Altitude Multiple Altimeter Beam Experimental Lidar (MABEL)," J. Coast. Res. 76(SI), 44–55 (2016).

[26] J. Morison, D. Hancock, S. Dickinson, J. Robbins, L. Roberts, R. Kwok, S. P. Palm, B. Smith, M. F. Jasinski, and the ICESat-2 Science Team, "ATLAS/ICESat-2 L3A Ocean Surface Height, Version 1," Boulder Colo. USA NASA Natl. Snow Ice Data Cent. Distrib. Act. Arch. Cent. (2019).

[27] X. Lu, Y. Hu, X. Zeng, S. A. Stamnes, T. A. Neuman, N. T. Kurtz, Y. Yang, P.-W. Zhai, M. Gao, W. Sun, K. Xu, Z. Liu, A. H. Omar, R. R. Baize, L. J. Rogers, B. O. Mitchell, K. Stamnes, Y. Huang, N. Chen, C. Weimer, J. Lee, and Z. Fair, "Deriving Snow Depth From ICESat-2 Lidar Multiple Scattering Measurements: Uncertainty Analyses," Front. Remote Sens. 3, (2022).

[28] Y. Hu, X. Lu, X. Zeng, S. A. Stamnes, T. A. Neuman, N. T. Kurtz, P. Zhai, M. Gao, W. Sun, K. Xu, Z. Liu, A. H. Omar, R. R. Baize, L. J. Rogers, B. O. Mitchell, K. Stamnes, Y. Huang, N. Chen, C. Weimer, J. Lee, and Z. Fair, "Deriving Snow Depth From ICESat-2 Lidar Multiple Scattering Measurements," Front. Remote Sens. 3, (2022).

[29] R. Kwok, S. Kacimi, M. A. Webster, N. T. Kurtz, and A. A. Petty, "Arctic Snow Depth and Sea Ice Thickness From ICESat-2 and CryoSat-2 Freeboards: A First Examination," J. Geophys. Res. Oceans 125(3), e2019JC016008 (2020).

[30] X. Lu, Y. Hu, Y. Yang, P. Bontempi, A. Omar, and R. Baize, "Antarctic spring ice-edge blooms observed from space by ICESat-2," Remote Sens. Environ. 111827 (2020).

[31] X. Lu, Y. Hu, and Y. Yang, "Ocean Subsurface Study from ICESat-2 Mission," in 2019 Photonics & Electromagnetics Research Symposium - Fall (PIERS - Fall) (2019), pp. 910–918.

[32] T. A. Neumann, A. Brenner, D. Hancock, J. Robbins, J. Saba, K. Harbeck, A. Gibbons, J. Lee, S. B. Luthcke, and T. Rebold, "ATLAS/ICESat-2 L2A Global Geolocated Photon Data, Version 5," Boulder, Colorado USA. NASA National Snow and Ice Data Center Distributed Active Archive Center. (2021).

[33] M. Vaughan, M. Pitts, C. Trepte, D. Winker, P. Detweiler, A. Garnier, B. Getzewich, W. Hunt, J. Lambeth, K.-P. Lee, P. Lucker, T. Murray, S. Rodier, T. Tremas, A. Bazureau, and J. Pelon, "Cloud – Aerosol LIDAR Infrared Pathfinder Satellite Observations (CALIPSO) Data Management System Data Products Catalog," Document No: PC-SCI-503(Release 4.92), (2020).

[34] https://asdc.larc.nasa.gov/project/CALIPSO

[35] https://nsidc.org/data/ATL03

[36] T. Neumann, A. Brenner, D. Hancock, J. Robbins, J. Saba, and K. Harbeck, "ICE, CLOUD, and Land Elevation Satellite - 2 (ICESat-2) Project Algorithm Theoretical Basis Document (ATBD) for Global Geolocated Photons ATL03," NASA Goddard Space Flight CenterGreenbelt Md. (2018).

[37] J. Kar, M. A. Vaughan, K.-P. Lee, J. L. Tackett, M. A. Avery, A. Garnier, B. J. Getzewich, W. H. Hunt, D. Josset, Z. Liu, P. L. Lucker, B. Magill, A. H. Omar, J. Pelon, R. R. Rogers, T. D. Toth, C. R. Trepte, J.-P. Vernier, D. M. Winker, and S. A. Young, "CALIPSO lidar calibration at 532 nm: version 4 nighttime algorithm," Atmos Meas Tech 11(3), 1459–1479 (2018).

[38] B. J. Getzewich, M. A. Vaughan, W. H. Hunt, M. A. Avery, K. A. Powell, J. L. Tackett, D. M. Winker, J. Kar, K.-P. Lee, and T. D. Toth, "CALIPSO lidar calibration at 532 nm: version 4 daytime algorithm," Atmos Meas Tech 11(11), 6309–6326 (2018).

[39] X. Lu, Y. Hu, A. Omar, Y. Yang, M. Vaughan, S. Rodier, A. Garnier, R. Ryan, B. Getzewich, and C. Trepte, "Nearshore bathymetry and seafloor property studies from Space lidars: CALIPSO and ICESat-2," Optics Express, under review. (2022).

[40] M. J. Behrenfeld, Y. Hu, K. Bisson, X. Lu, and T. K. Westberry, "Retrieval of ocean optical and plankton properties with the satellite Cloud-Aerosol Lidar with Orthogonal Polarization (CALIOP) sensor: Background, data processing, and validation status," Remote sensing of Environment, Under review. (2022).

[41] C. Cox and W. Munk, "Measurement of the Roughness of the Sea Surface from Photographs of the Sun's Glitter," J. Opt. Soc. Am. 44(11), 838–850 (1954).

[42] Hu, K. Stamnes, M. Vaughan, J. Pelon, C. Weimer, D. Wu, M. Cisewski, W. Sun, P. Yang, B. Lin, A. Omar, D. Flittner, C. Hostetler, C. Trepte, D. Winker, G. Gibson, and M. Santa-Maria, "Sea surface wind speed estimation from space-based lidar measurements," Atmos Chem Phys 8(13), 3593–3601 (2008).

[43] F. J. Wentz, T. Meissner, C. Gentemann, K. A. Hilburn, and J. Scott, "Remote Sensing Systems GCOM-W1 AMSR2 Monthly Environmental Suite on 0.25 deg grid, Version V.8.2," Remote Sens. Syst. St. Rosa CA (2014).